AIAA JOURNAL
Vol. 44, No. 4, April 2006

Large-Eddy Simulations as a Design Tool for Gas Turbine Combustion Systems

S. James,* J. Zhu,† and M. S. Anand‡
Rolls–Royce, Indianapolis, Indiana 46206

In recent years, large-eddy simulation (LES) has emerged as a promising next-generation computational tool for design applications. Compared to Reynolds-averaged Navier–Stokes simulation, the advantages that LES offers, in terms of improved turbulent mixing and ability to predict unsteady phenomena, makes it attractive for gas turbine combustor applications. An overview of recent activities related to LES being pursued at Rolls–Royce is provided. The LES methodology is reviewed both from numerical and modeling perspectives. The state of the art in subgrid-scale (SGS) modeling and spray modeling is discussed. Recently developed SGS reaction-rate closures such as the transport filtered density function method are reviewed and discussed. Validation experiments performed on several benchmark flows (nonreacting and reacting) and practical gas turbine combustor configurations are presented. Finally, ongoing developments for improving the LES methodology are highlighted.

Nomenclature

$\langle A \rangle$ = expected value of A
$\langle A|B \rangle$ = expected value of A conditioned on B
B_m = mass transfer number
B_T = heat transfer number
C = standard Smagorinsky constant
C_D = coefficient of drag of a spray particle
C_k = turbulent-viscosity constant in the one-equation kinetic-energy model
C_ε = dissipation term constant in the one-equation kinetic-energy model
C_ϕ = model constant in the Interaction by exchange with the mean model
c_{p_g} = gas-phase specific heat coefficient at constant pressure
c_{pp} = specific heat capacity of a droplet
D = molecular diffusivity
D_T = turbulent diffusivity
d^k = diameter of the kth spray particle
F_L = filtered mass density function
G = filter kernel
J_i^α = diffusional flux of species α in the ith-coordinate direction
k = turbulent kinetic energy
k_g = gas-phase thermal conductivity
k_{sgs} = subgrid scale kinetic energy
M_i^α = subgrid scale mass flux of scalar α
$\dot{m}_p$ = rate of change of mass of a spray particle
p = pressure
Re^k = Reynolds number of the kth spray particle
Sc_t = turbulent Schmidt number
$\underline{S_{ij}}$ = strain-rate tensor
$\overline{S_m}$ = spray source term in the continuity equation
$\overline{S_{mi}}$ = spray source term in the momentum equation
$\overline{S_{m\alpha}}$ = spray source term in the scalar transport equation
S_α = chemical source term of species α
$\tilde{S}_\alpha$ = filtered reaction rate of scalar α
T_{ij} = subgrid stress tensor
u_i = instantaneous velocity in the ith-coordinate direction
$\tilde{u}_i$ = Favre filter of u_i
V_i^k = velocity of the kth spray-particle in the ith-coordinate direction
x_i = Cartesian coordinate in the i direction
Δ = filter width
δ = Dirac delta function
δ_{ij} = Kronecker delta
ε = turbulent dissipation
μ (or μ_g) = gas-phase molecular viscosity
μ_T = turbulent viscosity
ν_T = turbulent kinematic viscosity
ξ = instantaneous mixture fraction
ρ (or ρ_g) = gas-phase density
ρ_p = density of a spray particle
$\bar{\rho}$ = filtered (or mean) density
τ_d = spray particle relaxation time
$\overline{\tau_{ij}}$ = filtered viscous stress tensor
ϕ_α = mass fraction of species α in physical space
$\bar{\phi}$ = filtered value of a scalar ϕ
ψ_α = mass fraction of species α in composition space
ω = mixing frequency

Received 4 January 2005; revision received 24 October 2005; accepted for publication 26 October 2005.

*Specialist, P.O. Box 420, Speed Code T-14, Combustion Systems. Member AIAA.
†Senior Specialist, P.O. Box 420, Speed Code T-14, Combustion Systems.
‡Group Leader/Consultant, P.O. Box 420, Speed Code T-14, Combustion Systems. Member AIAA.

Introduction

THERE are three main avenues to computing turbulent reacting flows: Reynolds-averaged Navier–Stokes simulations (RANS), large-eddy simulations (LES), and direct numerical simulations (DNS). In the gas turbine industry, RANS is the primary means of analyzing combusting flows, mainly due to its relatively fast turnaround time and success in providing design guidance for meeting exit temperature profile requirements. RANS has also been used to predict emissions, but such predictions have met with mixed success. Predictions are also known to be sensitive to the turbulence model used. For example, when both the liner and annuli of a gas turbine combustor are included in the computational flow model, the standard k–ε model predicts incorrect turbulence levels at the primary and dilution ports of the liner. At the other extreme, DNS is computationally affordable only for simple configurations at low Reynolds numbers and is mainly a tool to validate turbulence and combustion submodels for RANS and LES. At high Reynolds numbers, the enormous grid resolution requirement makes DNS unaffordable for practical applications. LES is also computationally intensive, however, to a lesser degree than DNS. Unlike in DNS, where all length scales and timescales are resolved, only large-scale structures are directly resolved in LES. The small scales are modeled.

With the availability of powerful computers and distributed computing platforms, increasing applications of LES to complex geometries are being reported in literature.[1–4] LES is now considered to be the next-generation practical design tool for gas turbine combustors. With low emissions being an important aspect of combustor design, it is becoming increasingly important to overcome new technological barriers to combustor design such as combustion instabilities. RANS-based tools cannot provide insight into these phenomena. LES, due to its time-accurate nature, may be used to understand and predict these instabilities. Additionally, combustion mainly occurs away from walls in gas turbine combustors; therefore, sophisticated wall treatments are not required, a favorable feature for LES.

For LES to be a reliable combustion design tool, extensive validations of various submodels used in the methodology are required. Numerics play an important role in LES, and close attention has to be paid to the numerical scheme used. In this paper, the LES methodology for application to complex configurations is reviewed. Both numerical and modeling aspects of the methodology are examined. The state of the art in subgrid-scale modeling and liquid-fuel spray modeling for LES is presented and discussed. A hierarchy of validation cases performed on several nonreacting and reacting benchmark flows are presented. These cases, ranging from simple lid-driven cavity flow to complex gas turbine combustor flow, highlight the predictive capabilities of LES.

Theoretical and Numerical Aspect of LES

In LES, the most energetic flow structures are directly resolved, whereas the small-scale flow structures are modeled. The instantaneous numerical solution from LES represents an instantaneous realization of the turbulent flow with frequencies above a certain cutoff value filtered out. This is in contrast to RANS, which produces a time average of the turbulent flow. LES also affords advantages over RANS in modeling aspects. Small-scale structures are not significantly affected by inhomogeneities; therefore, it is believed that modeling these structures is less daunting than the modeling that accounts for all scales as in RANS.

Filtering Operation

The large-scale or filtered field can be mathematically expressed as[5]

$$\bar{\phi}(\boldsymbol{x}, t) = \frac{1}{\Delta}\int_{-\infty}^{+\infty} \phi(\boldsymbol{x}', t)\, G\left(\frac{|\boldsymbol{x} - \boldsymbol{x}'|}{\Delta}\right) \mathrm{d}\boldsymbol{x}' \tag{1}$$

where $\phi(\boldsymbol{x}', t)$ is the instantaneous field and G is a localized filter kernel with filter width Δ having the following properties:

$$\int_{-\infty}^{+\infty} G(\psi)\, \mathrm{d}\psi = 1 \tag{2a}$$

$$G(-\psi) = G(\psi) \tag{2b}$$

$$\int_{-\infty}^{+\infty} x^m G(\psi)\, \mathrm{d}\psi \qquad \text{exist for } m \geq 0 \tag{2c}$$

Examples of filters include a box filter, a Gaussian filter, and a Fourier cutoff filter (see Ref. 6). An interpretation of Eq. (1) is that the mean (or filtered) field is constructed from an instantaneous field by filtering eddies of size smaller than Δ.

Governing Equations

Applying the filtering operation to the instantaneous transport equations, we obtain the following:

$$\frac{\partial \bar{\rho}}{\partial t} + \frac{\partial \bar{\rho}\tilde{u}_i}{\partial x_i} = \overline{S_m}$$

$$\frac{\partial \bar{\rho}\tilde{u}_j}{\partial t} + \frac{\partial \bar{\rho}\tilde{u}_i\tilde{u}_j}{\partial x_i} = -\frac{\partial \bar{p}}{\partial x_j} + \frac{\partial \overline{\tau_{ij}}}{\partial x_i} - \frac{\partial T_{ij}}{\partial x_i} + \overline{S_{mj}}$$

$$\frac{\partial \bar{\rho}\tilde{\phi}_\alpha}{\partial t} + \frac{\partial \bar{\rho}\tilde{u}_i\tilde{\phi}_\alpha}{\partial x_i} = -\frac{\partial}{\partial x_i}\left(\bar{\rho}\tilde{D}\frac{\partial \tilde{\phi}_\alpha}{\partial x_i}\right) - \frac{\partial M_i^\alpha}{\partial x_i} + \bar{\rho}\tilde{S}_\alpha + \overline{S_{m\alpha}} \tag{3}$$

where ρ is the density, τ_{ij} is the viscous stress tensor, and ϕ_α is the scalar array, $T_{ij} = \overline{\rho u_i u_j} - \bar{\rho}\tilde{u}_i\tilde{u}_j$ and $M_i^\alpha = \overline{\rho u_i \phi_\alpha} - \bar{\rho}\tilde{u}_i\tilde{\phi}_\alpha$ denote the subgrid-scale (SGS) stress and SGS scalar mass flux, respectively. $\tilde{S}_\alpha$ are the filtered reaction source terms. $\overline{S_m}$, $\overline{S_{mi}}$, and $\overline{S_{m\alpha}}$ are the liquid fuel source terms in the continuity, momentum, and scalar equations, respectively. Note that in the preceding equations, quantities with the tilde represent Favre-average filters.

In most LES, the filtering operation is not explicitly performed in simulations. Instead, it is argued that the discretization scheme for derivatives and the finite spectral support of the computational grid (where only wave numbers smaller than $\pi/\Delta x$ can be represented on a grid with spacing Δx) mimic the filtering operation. This is commonly referred to as implicit filtering. The filter width in the implicit filtering approach is typically assumed to be the local grid spacing. An assumption implied in the derivation of Eq. (3) is that the filtering operation commutes with spatial differentiation, that is, $\overline{\partial\phi/\partial x} = \partial\bar{\phi}/\partial x$. However, this is not true in the case when nonuniform grids are used. Nevertheless, the error incurred due to loss of commutative property is second order in the filter width.[7] Hence, in most LES applications employing second-order schemes, this error is typically neglected. A consequence of linking the filter width to the grid spacing is that, as the grid is refined, the filter width also becomes smaller. Consequently, more scales are resolved in the flowfield and the contribution of the SGS model becomes smaller. Eventually, the LES simulation converges to a DNS as the grid size is made smaller and smaller.

Numerical Method

Equation (3) can be solved by a density-based or a pressure-based method. In the RANS context, the pressure-based method has been widely used for simulating gas turbine combustor flows.[8] The density-based method can also be applied to such flows; however, appropriate preconditioners have to be used to avoid time-step restrictions imposed by the low-speed flow.

Robustness and low numerical dissipation of the numerical scheme are issues of utmost importance in LES of gas turbine combustors. For RANS applications in complex geometries, upwind-type methods are typically used and have been known to produce reasonable results. However, studies[9] have shown that these methods when applied to LES simulations show undue damping of small-scale structures. Central differencing schemes are typically preferred[9] because these schemes do not exhibit numerical dissipation. A drawback of these schemes is that computations are sensitive to nonuniformities in the grid. Grids, therefore, have to be constructed with care. However, even with the utmost care, grid spacing can vary quite rapidly in regions near the fuel nozzle of gas turbine combustors, triggering numerical instabilities in LES.

A means to enhance the robustness of LES simulations on such grids is to ensure discrete kinetic energy conservation.[10–14] In the inviscid limit (or high-Reynolds-number flows) and in the absence of time-discretization errors, kinetic energy, defined as $u_i u_i/2$, is considered to be discretly conserved if the numerical approximation of all of the terms in its transport equation can be expressed in divergence form. This implies that, in a computational domain with periodic boundaries, the numerical scheme will force the total kinetic energy of the system to be constant at all times (as expected). Numerical methods that employ central difference schemes but do not satisfy energy conservation are often unstable at high Reynolds numbers. Discrete kinetic energy conservation in staggered and collocated numerical schemes has been investigated in detail by Morinishi et al.[10] Because of their simplicity, collocated schemes are usually preferred over staggered schemes for simulating flows in complex geometries. In collocated schemes, the cell-face fluxes are typically computed using a procedure outlined by Rhie and Chow.[15] This procedure, although preventing checkerboarding of the pressure field, results in violation of discrete kinetic-energy conservation. The impact of this violation has not been extensively studied, but limited studies performed by Benhamadouche et al.[13] suggest that it may not be serious. Kinetic-energy conservation is also lost when cell-face quantities are computed by weighted interpolations.[11] This is not an issue when uniform grids are used.

However, the problem can be easily overcome by using a symmetric interpolation scheme.[11,12,14]

Assessing the convergence of LES solutions is an issue that has not been given importance by LES practitioners. A grid-independent instantaneous field cannot be achieved in LES, because the filter width is linked to the local grid spacing. However, in most LES studies, one is interested in time-averaged quantities, which can be shown to be grid independent by refining the grid. Hence, when assessing different submodels, the model that provides optimal accuracy at a minimum computational cost could be considered as superior. More details on appraising LES are discussed by Pope.[16]

The LES method used for simulations presented in this paper is implemented in the Rolls–Royce corporate combustion design analysis system, PRECISE. The LES solver is based on a collocated, finite volume, structured-grid, incompressible, pressure-based method.[8] Spatial derivatives for velocities are discretized by a second-order central scheme. For the scalar fields, the hybrid or the hybrid-linear parabolic approximation scheme[17] is typically used to ensure boundedness of scalars. Time derivatives are discretized by a second-order backward difference scheme. A SIMPLE-type[18] method is used to converge the discretized equations at each time step. For reacting flows, roughly 10 iterations suffice for convergence at each time step.

Modeling

In Eq. (3), the unclosed terms are SGS stress, SGS scalar flux, and filtered reaction rates. For liquid fuels, additional modeling of spray source terms is required. In the following sections, we will review models for these terms and present some sample results.

SGS Stress and Scalar Flux

The majority of SGS stress models are based on the eddy-viscosity approach. Since the early pioneering work by Smagorinsky,[19] there have been several variants[20–24] of the eddy viscosity model that have shown improved predictive capabilities.

The Smagorinsky model is given by the expression

$$T_{ij} - (\delta_{ij}/3)T_{kk} = -2\nu_T \tilde{S}_{ij} = -2(C\Delta)^2|\tilde{S}|\tilde{S}_{ij} \tag{4}$$

where $\tilde{S}_{ij} = \frac{1}{2}(\partial\tilde{u}_i/\partial x_j + \partial\tilde{u}_j/\partial x_i)$ is the strain rate tensor, ν_T is the turbulent viscosity, and $|\tilde{S}|$ is the magnitude of the strain rate tensor. The filter width Δ is typically considered to be the local grid spacing. In the standard Smagorinsky model, the constant C is assumed to have a fixed value. A review of literature shows significant variation in the value used for C; values ranging from 0.065 to 0.17 have been used.

The dynamic model proposed by Germano et al.[20] overcomes the limitation of tuning the constant C. In this model, C is computed dynamically via an identity that relates stresses at different scales. There are several variants of the dynamic model that provide improved predictions, for example, the localized dynamic model,[21] the dynamic localization model,[22] the Lagrangian dynamic model (see Ref. 23), and scale-dependent dynamic model.[24]

Another class of SGS stress models is based on the one-equation model, in which the transport equation for the SGS turbulent kinetic energy equation is solved.[25] It has been argued that by solving this equation, the equilibrium assumption, that is, production equals dissipation of SGS kinetic energy, inherent in algebraic eddy-viscosity models, is no longer required. Therefore, a relatively coarser grid could be used. The SGS kinetic energy equation is defined as

$$k_{\text{sgs}} = \tfrac{1}{2}(\widetilde{u_k u_k} - \tilde{u}_k\tilde{u}_k) \tag{5}$$

and its transport equation can be derived to be

$$\frac{\partial\bar{\rho}k_{\text{sgs}}}{\partial t} + \frac{\partial}{\partial x_j}(\bar{\rho}\tilde{u}_i k_{\text{sgs}}) = P_{\text{sgs}} - D_{\text{sgs}} + \frac{\partial}{\partial x_i}\left(\frac{\overline{\rho}\nu_t}{Pr_t}\frac{\partial k_{\text{sgs}}}{\partial x_i}\right) \tag{6}$$

The terms on the right-hand side represent production, dissipation, and transport of the subgrid kinetic energy, respectively. Here, the production term is

$$P_{\text{sgs}} = -T_{ij}\left(\frac{\partial\tilde{u}_i}{\partial x_j}\right) \tag{7}$$

The SGS stress is modeled as

$$T_{ij} = -2\bar{\rho}C_k\Delta k_{\text{sgs}}^{\frac{1}{2}}\left(\tilde{S}_{ij} - \tfrac{1}{3}\tilde{S}_{kk}\delta_{ij}\right) + \tfrac{2}{3}\bar{\rho}k_{\text{sgs}}\delta_{ij} \tag{8}$$

where the turbulent viscosity is defined as $\nu_t = C_k\Delta k_{\text{sgs}}^{1/2}$. The dissipation term is modeled as

$$D_{\text{sgs}} = C_\varepsilon\bar{\rho}k^{\frac{3}{2}}/\Delta \tag{9}$$

The two parameters C_k and C_ε are assumed to be either a constant or computed dynamically.

To illustrate the predictive capability of the eddy-viscosity model, an assessment of RANS with the k–ε model and LES with standard Smagorinsky model, localized dynamic model, and one-equation kinetic-energy equation model is performed for the flow in a lid-driven, three-dimensional cavity. The value of the constant C in the standard Smagorinsky model is set to 0.17. In the kinetic-energy equation model, a dynamic procedure is used to compute C_k, but a constant value of 0.916 is used for C_ε. The flow configuration consists of a three-dimensional cavity bounded by walls with the upper wall (or lid) moving at a velocity U_B. Fluid motions are generated by shear stresses at the moving wall. Past studies have shown that at a Reynolds number Re lower than 5×10^3 the flow is essentially laminar with inherent unsteadiness. At $Re > 6 \times 10^3$, the flow becomes unstable near the downstream eddy and at $Re > 1 \times 10^4$, the flow near the downstream eddy becomes fully turbulent. The experimental data used for comparisons with the present LES calculations were collected by Prasad and Koseff.[26] Data were collected for three different Reynolds numbers at different spanwise aspect ratios (SAR), defined as L/B, where L is the cavity span and B is the breadth of the cavity. Simulations are conducted for $Re = 1 \times 10^4$ and SAR $= 0.5$ with a mesh resolution of $64 \times 64 \times 32$. Figure 1 presents the mean streamwise, u, and transverse, v, velocities from the three simulations at the spanwise midplane of the cavity. It can be seen that the predictions using the dynamic and one-equation models show very good agreement with data. RANS shows poor agreement with data. The standard Smagorinsky model shows an improvement over RANS; however, predictions are not as good as those from the other LES models. This is even more apparent in Fig. 2, which shows the rms of u and v velocities at the same plane. The dynamic and one-equation models show reasonable agreement with data, whereas the

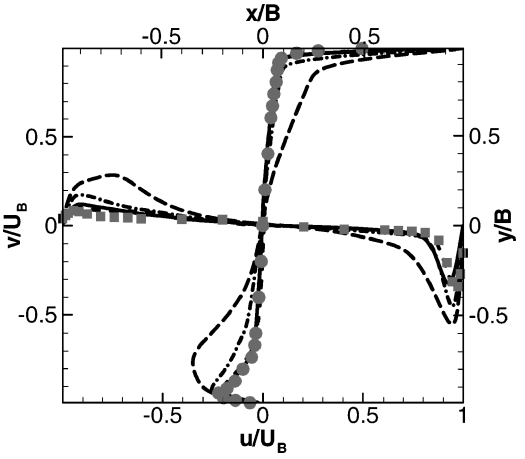

Fig. 1 Comparison of mean u and v velocities with experimental data for lid-driven cavity flow using various models: ——, localized dynamic; - - - -, kinetic-energy equation; —·—, standard Smagorinsky; — —, RANS; ●, experimental data for u velocity; and ■, experimental data for v velocity.

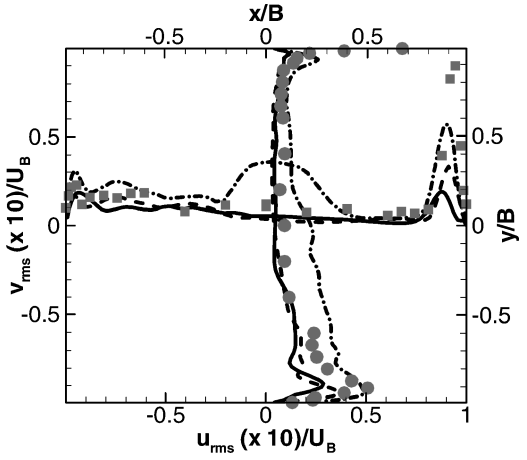

Fig. 2 Comparison of turbulence intensities with experimental data for lid-driven cavity flow various models: ——, localized dynamic; - - - -, kinetic-energy equation; —·—, standard Smagorinsky; ●, experimental data for u velocity; and ■, experimental data for v velocity.

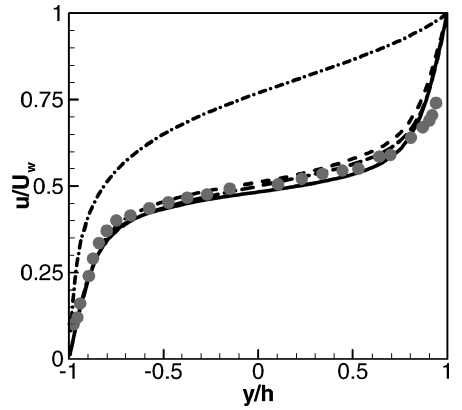

Fig. 3 Comparison of mean u velocity using dynamic and kinetic-energy models with DNS and experimental data for plane turbulent Couette flow: ——, localized dynamic; - - - -, kinetic-energy equation; — —, DNS data of Bech et al.[27]; —·—, RANS (note wall functions not used at moving wall); and ●, experimental data of Aydin and Leutheusser.[28]

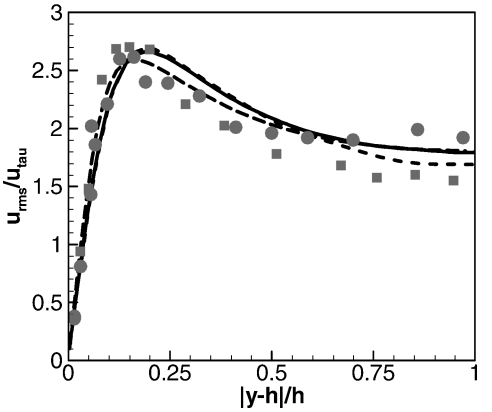

Fig. 4 Comparison of rms of u velocity using dynamic and kinetic-energy models with DNS and experimental data for plane turbulent Couette flow: ——, localized dynamic model; - - - -, kinetic-energy model; — —, DNS data of Bech et al.[27]; ■, experimental data of Bech et al.[27]; and ●, experimental data of Aydin and Leutheusser.[28]

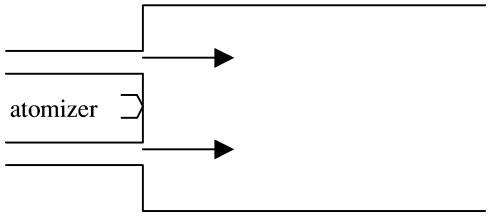

Fig. 5 Schematic of Sommerfeld and Qiu[29] experimental configuration.

standard Smagorinsky model shows significant deviation from the data. It may be possible to improve the predictions of the standard Smagorinsky model by tuning the constant C.

Results from LES of a plane turbulent Couette flow are shown in Figs. 3 and 4. This flow is essentially driven by shear generated by the relative motion of two parallel plates. Physical experiments on this flow configuration were performed by Bech et al.[27] and Aydin and Leutheusser.[28] Bech et al.[27] also performed DNS of this flow. In the present simulations, the upper wall has a fixed velocity U_w, whereas the lower wall is fixed. Periodic boundary conditions are imposed in the axial and spanwise directions. The transitional Reynolds number for plane Couette flows is approximately 300 and fully developed turbulence is achieved at Reynolds numbers above 500. For the present study, the Reynolds number is $Re = 2.6 \times 10^3$; the flow is, therefore, fully turbulent. The computational domain has dimensions $4\pi h \times 2h \times 2\pi h$ in the streamwise, normal, and spanwise directions, where h is the channel half-height. A grid resolution of $32 \times 32 \times 32$ grid is used in the simulations. As in the cavity case, simulations of the Couette flow are performed with the localized dynamic and one-equation models. Figure 3 presents the mean streamwise velocities in the spanwise midplane. The predictions are in good agreement with both experimental data and DNS simulation. Note that RANS shows a very different prediction. In the RANS simulation, no wall functions are used at the moving wall and, therefore, may be a cause for the poor prediction. In the LES simulations, no wall functions are imposed. Figure 4 shows rms of the streamwise velocity normalized by the wall-shear velocity. It can be seen that the LES predictions are in reasonable agreement with data and DNS. The turbulent kinetic energy in RANS (not shown) does not show the same behavior.

The third test case presented is the experiment of Sommerfeld and Qiu.[29] The flow configuration, shown in Fig. 5, is more complex than the preceding two cases. Heated air is blown from an annular injection tube into a test section that has an inner diameter of 200 mm and a length of 1500 mm. The inner and outer diameters of the annulus are 40 and 64 mm, respectively. The air mass flow rate is 29 g/s, and the air temperature is 373 K. A hollow cone pressure atomizer is mounted in the cylindrical centerbody of the inlet tube. A set of measurements obtained without the atomizer in operation is used to validate LES of this flow configuration. The localized dynamic model is used in the simulations.

The computational domain is constructed entirely by H-elements and consists of 9 blocks. A total of 1.2 million grid points are used to represent the flow domain. To take advantage of parallel processing capabilities, the domain is decomposed into five subdomains. Each subdomain is acted on by an independent processor. A laminar profile is used at the inlet and full-developed conditions are assumed at the exit boundary. No perturbations are imposed on the inlet profile. Instantaneous contours of u velocity are shown in Fig. 6. As reported in the experiments, a small recirculation region is seen in front of the atomizer, and the recirculation region at the edge of the pipe expansion extends throughout the flow domain. Figure 7 shows a comparison of the prediction of mean u velocity against data at several axial locations. It can be seen that the predictions are in reasonable agreement with data. Figure 8 presents the rms of u velocity at the same axial stations. Again, the rms predictions are also in reasonable agreement with the data.

The preceding three cases show that the localized dynamic and one-equation kinetic-energy models are able to predict the flowfield reasonably without having to tune boundary conditions. A third class of subgrid stress models proposed in literature is scale-similarity models. In this model, the unfiltered velocity in the SGS stress terms is approximated by the filtered velocity.[30] However,

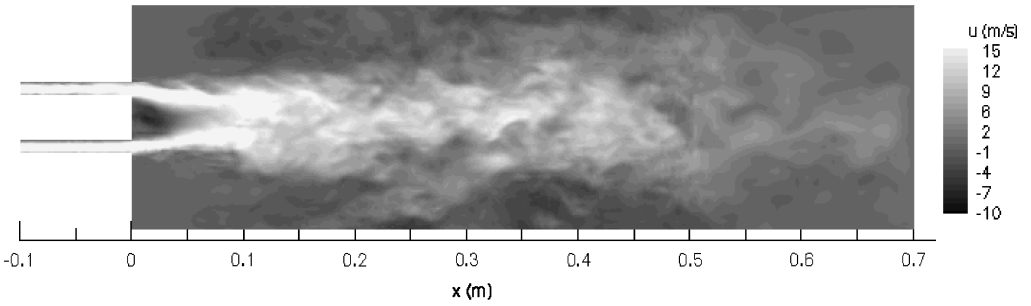

Fig. 6 Instantaneous u-velocity contours in Sommerfeld and Qiu[29] experiment study.

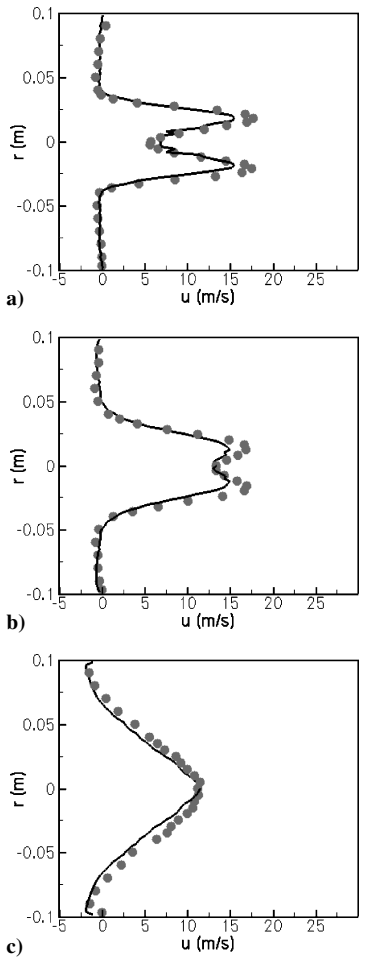

Fig. 7 Comparison of mean u velocity at several axial locations in Sommerfeld and Qiu[29] experiment: a) $x = 0.05$ m, b) $x = 0.1$ m, and c) $x = 0.3$ m: ——, computations and ●, experimental data.

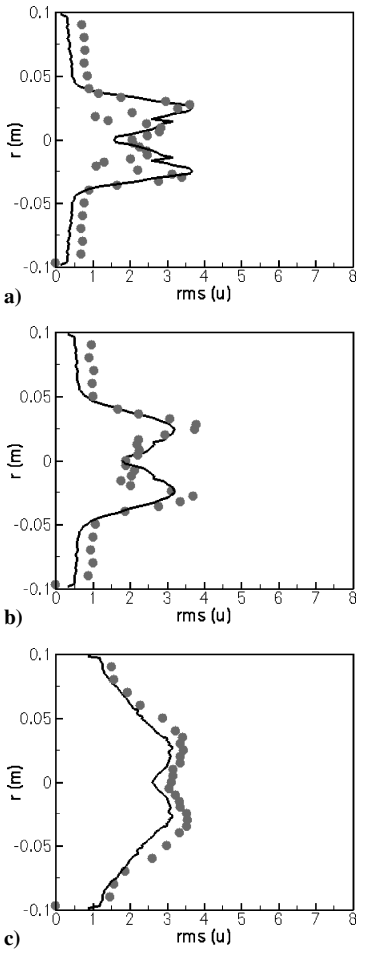

Fig. 8 Comparison of rms of u velocity at several axial locations in Sommerfeld and Qiu[29] experiment: a) $x = 0.05$ m, b) $x = 0.1$ m, and c) $x = 0.3$ m: ——, computations and ●, experimental data.

simulations based on this model suffer from lack of sufficient dissipation and the model has to be supplemented by an eddy-viscosity model to stabilize the calculations.[31] A fourth category of subgrid stress models is based on the idea of reconstructing the unresolved primitive variables and directly computing the stresses from their defining equations. The approximate deconvolution model[32] and the SGS estimation model[33] fall in this category. These models are yet to be tested in complex reacting flow configurations. For a detailed exposition on SGS stress models, the reader may refer to recent review articles.[34,35]

The most widely used model for closure of the SGS scalar flux term is the gradient diffusion model[36–42] given by the expression

$$M_\alpha^i = -\bar{\rho} D_t \frac{\partial \tilde{\phi}_\alpha}{\partial x_i} \tag{10}$$

where $D_t = \nu_t / Sc_t$. The turbulent Schmidt number can be either assumed to be a constant or computed dynamically.[42] The SGS stress and scalar flux terms can be computed exactly when the transport equation of the joint filtered density function (FDF) of velocity and scalars is solved.[43] However, there are other unclosed terms in the joint FDF transport equation for which appropriate models have to be devised.

Spray Modeling

The spray methodology that is typically used in LES is for the most part adopted from RANS applications.[8] The Lagrangian method with two-way coupling is the most common approach used to simulate droplet dynamics. The dispersed phase is represented by computational particles with no particle–particle interactions. Each computational particle is a representation of a group of actual spray particles having the same size, velocity, and temperature. To represent the spray physics, spray tracking and evaporation processes need to be modeled accurately. In RANS, because time accuracy is usually not important, each computational particle is tracked until it

completely evaporates or leaves the computational domain, before another particle is injected. In LES, due to the constraint of time accuracy, several particles are injected from the fuel nozzle and tracked for the duration of the time step. Subsequently, more particles are injected from the fuel nozzle and the process repeated. Hence, at a given instant of time, there may be a large number of particles in the flow domain.

The governing equation of motion for the kth particle in the i direction is given by[44]

$$\frac{\mathrm{d}V_i^k}{\mathrm{d}t} = \frac{\left(u_i - V_i^k\right)}{\tau_d} \tag{11}$$

where

$$\tau_d = \frac{4d^k \rho_p}{3C_D \rho_g |\boldsymbol{u} - \boldsymbol{V}^k|} \tag{12}$$

In Eqs. (11) and (12), $\boldsymbol{u}$ is the instantaneous gas-phase velocity at the particle location and $\boldsymbol{V}^k$ is velocity of the kth particle. C_D is the drag coefficient, and and ρ_p and ρ_g are densities of the particle phase and gas phase, respectively. C_D is computed through nonlinear relationships[45] that are dependent on the particle Reynolds number, defined as

$$Re^k = \rho_p |\boldsymbol{u} - \boldsymbol{V}^k| d^k \big/ \mu_g \tag{13}$$

Note that instantaneous gas-phase velocities are needed in Eqs. (11–13). The standard approach in RANS is to use the turbulent kinetic energy to reconstruct the fluctuating velocities. A similar approach was used by Pannala and Menon,[46] where they used the SGS kinetic energy to reconstruct the unknown velocities. Studies by Miller and Bellan[47] showed that neglecting the subgrid velocity fluctuations results in erroneous predictions of the droplet drag force. Apte et al.[48] performed LES of swirling particle-laden flow in a coaxial-jet combustor without accounting for these fluctuations. Their predictions were in good agreement with data.

The commonly used evaporation model, to mimic heat and mass transfer from spray droplets, is based on a quasi-steady analysis of an isolated droplet in a quiescent environment.[49] The rate of change of mass of a particle is defined as

$$\dot{m}_p = 2\pi d^k (k/c_p)_g \ln(1 + B_m) \tag{14}$$

where k and c_p are the thermal conductivity and the specific heat capacity, respectively, of the gas phase. B_m is the mass transfer number.[49] The rate of change of drop surface temperature is given by

$$\frac{\mathrm{d}T_s}{\mathrm{d}t} = \frac{\dot{m}_p L}{c_{pp} m}\left[\frac{B_T}{B_m} - 1\right] \tag{15}$$

where L is the latent heat of fuel vaporization and B_T is the heat transfer number.[49] The effects of convection on heat and mass transfer rates can be accommodated by a correction factor, which is a function of Reynolds number and Schmidt (or Prandtl) number (see Ref. 49).

Modeling the inlet conditions for the spray injection process is another issue that is equally important. The common procedure is to inject spray size groups from a Rossin–Rammler distribution (e.g., see Ref. 50). More recent approaches are based on modeling the primary breakup of the liquid film issuing from the fuel nozzle, followed by a secondary breakup process (e.g., Refs. 51 and 52).

As an illustrative example, LES of an evaporating fluid in a turbulent airstream is performed for the flow configuration studied by Sommerfeld and Qiu.[29] The flow configuration is the same as that shown in Fig. 5. The hollow cone pressure atomizer issues isopropyl alcohol into the cylindrical tube. Detailed measurements of droplet particle velocities and diameters are available at several axial locations.[29] In the LES, spray droplets are injected around a ring with radius 3 mm. The cone angle of the spray is set to 60 deg (Ref. 29). Mean axial velocity is set to 18 m/s and Sauter mean diameter is set to 40. The fuel flow rate is 0.44 g/s, and the airflow rate is 28.3 g/s. At each time step, 10 spray droplet size groups are sampled from a modified Rossin–Rammler distribution (see Ref. 50). At the next time step another 10 spray droplet size groups (not the same as those in the previous time step) are sampled and so on. This procedure ensures that over a large number of time steps the droplet distribution is accurately mimicked. The key to performing accurate spray simulations is an accurate spray-tracking algorithm. The spray-tracking algorithm implemented in the LES code is the same as that implemented for tracking computational particles in the transport probability density function (PDF) method.[53] This algorithm, which is based on identifying cell-face crossings of particles, is quite robust even in complicated geometries. The spray-tracking algorithm has also been parallelized to take advantage of distributed computing. Figure 9 shows the spray particles in the computational domain at one instant of time. Large droplets are present in the near field of the spray nozzle and typically found at large radii. Farther downstream droplets evaporate and only smaller droplets are found. Figure 10 presents the mean particle velocities at several axial locations. Note that the predictions are in reasonable agreement with data. Figure 11 presents the mean particle diameters at several axial locations. Again, the predictions and the data match very well. Figure 11 also shows that large droplets are found at the edge of the spray, whereas small droplets are found in the core region. Far downstream of the inlet, particle diameters decrease and become more uniform due to evaporation. Ham et al.[52] also report similar predictions using an unstructured LES code.

Turbulent-Combustion Model

For applications of LES to turbulent reacting flows, appropriate turbulence–chemistry interaction model is required to close the reaction source terms [see Eq. (3)]. In the past decade, significant strides have been made in combustion modeling for LES. The majority of the models have been extensions of RANS models.

The eddy breakup model has been successfully used in reacting RANS simulations of gas turbine combustors.[8] The model has been extended for LES applications by Fureby and Lofstrom,[54] where they applied it to bluff-body stabilized flames. In this model, the mean reaction rate is assumed to be the minimum of the kinetically controlled reaction rate and the mixing controlled reaction rate. The

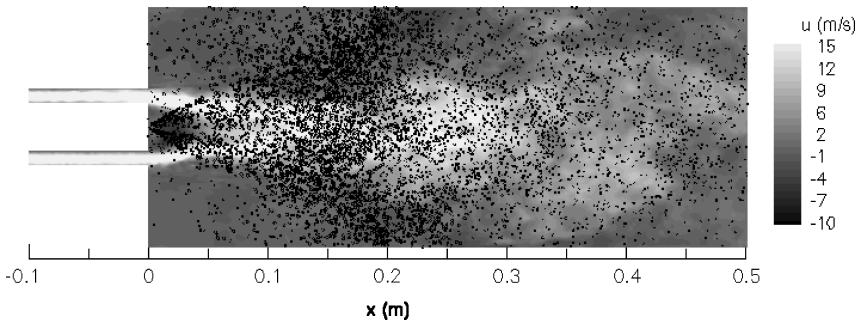

Fig. 9 Spray particles from LES simulation of Sommerfeld and Qiu[29] experiment superimposed on instantaneous u-velocity field.

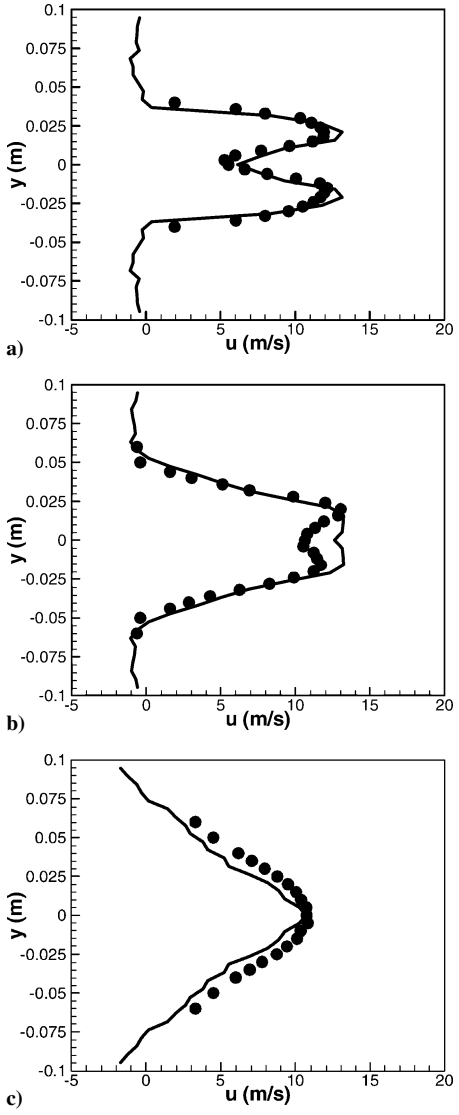

Fig. 10 Particle velocity predictions at several axial locations in Sommerfeld and Qiu[29] experiment: a) $x = 0.05$ m, b) $x = 0.1$ m, and c) $x = 0.3$ m: ●, experimental data and ——, LES predictions.

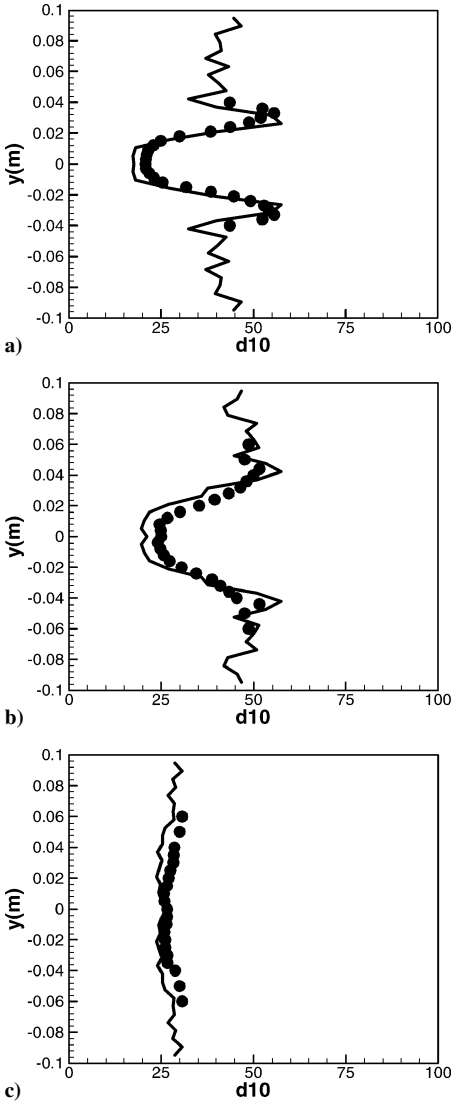

Fig. 11 Particle mean diameters at several axial locations in Sommerfeld and Qiu[29] experiment: a) $x = 0.05$ m, b) $x = 0.1$ m, and c) $x = 0.3$ m: ●, experimental data and ——, LES predictions.

mixing controlled rate is assumed to be proportional to the mixing frequency, computed based on the filter width and SGS kinetic energy.

More recently, flamelet models[37,55–57] based on single-variable and two-variable formulations have become popular. The advantage of flamelet-based approaches is that detailed chemical kinetics could be used to describe the flame. In the single-variable formulation, chemical species are functions of mixture fraction ξ only. The PDF of ξ is modeled as an assumed beta function, parameterized by the mean and variance of ξ. The mean value is computed from a transport equation, and the variance is computed from an algebraic relation, derived by assuming production equals dissipation in the variance transport equation.[57] In the two-variable formulation,[56] chemical species are functions of ξ and a reaction progress variable η. The PDF of η is typically assumed to be a Dirac-delta function. More recently,[58] other forms such as a beta PDF, parameterized by the mean and variance of η, have been assumed. Other SGS reaction models based on conditional moment closure[59] and closures for SGS stress terms[60,61] have also been proposed in literature.

A promising new development in subgrid reaction closures that avoids a priori specification of the PDF of scalars is the FDF transport method.[41,43,62–65] This method is analogous to the PDF transport method used in RANS simulations. In the scalar FDF transport method, a transport equation for the filtered mass density function (FMDF) is solved for. The FMDF is defined as

$$F_L(\psi, x; t) = \int_{-\infty}^{+\infty} \rho(x', t)\delta[\psi - \phi(x, t)]G(x' - x)\,\mathrm{d}x' \quad (16)$$

where δ is the delta function, ψ is the scalar variable in composition space, and G is the filter function. The transport equation for F_L can be derived to be of the form

$$\frac{\partial}{\partial t}(F_L) + \frac{\partial}{\partial x_i}(\langle u_i \rangle_i F_L) = \frac{\partial}{\partial \psi_\alpha}\left(\left\langle \frac{1}{\rho}\frac{\partial}{\partial x_i} J_i^\alpha \middle| \psi \right\rangle F_L\right)$$

$$-\frac{\partial}{\partial x_i}[(\langle u_i|\psi\rangle - \langle u_i\rangle)F_L] - \frac{\partial}{\partial \psi_\alpha}(S_\alpha F_L) \quad (17)$$

There are two terms in this equation that require modeling: the molecular mixing term (first term on the right-hand side) and the turbulent convection term (second term on the right-hand side). One of the mixing models used for the molecular mixing term is the interaction by exchange with the mean (IEM) model, given by

$$\frac{\partial}{\partial \psi_\alpha}\left(\left\langle \frac{1}{\rho}\frac{\partial J_i^\alpha}{\partial x_i} \middle| \psi \right\rangle F_L\right) = \frac{\partial}{\partial \psi_\alpha}[C_\phi \omega(\psi_\alpha - \langle \phi_\alpha \rangle)F_L] \quad (18)$$

A value of 2.0 is typically used for the model constant C_ϕ. The mixing frequency ω is expressed in terms of the SGS viscosity and

the filter size. The turbulent convection term is typically modeled by the gradient diffusion model given by

$$(\langle u_i|\psi\rangle - \langle u_i\rangle)F_L = -\langle\rho\rangle D_T \frac{\partial}{\partial x_i}\left(\frac{F_L}{\langle\rho\rangle}\right) \tag{19}$$

In Eq. (17), it can be seen that the last term on the right-hand side is due to chemical reactions and is in a closed form. Thus, reactions of arbitrary complexity could be used to describe chemical reactions. Given this advantage of the FDF method and also the fact that the PDF is not specified a priori as in flamelet models, it is expected that the LES/FDF method will yield better predictions of not only overall turbulent flame structures, but also local extinction and reignition scenarios in these flames.

The large dimensionality of Eq. (17) precludes the use of finite difference or finite volume schemes for the solution of this equation. The standard method to solve Eq. (17) is via Monte Carlo methods. In these methods, the FMDF in each computational cell is represented by an ensemble of notional particles, each with a set of scalars and position vector. The transport of these particles in physical and compositional space mimics the solution of Eq. (17). The mean velocities at the particle locations are computed by interpolating the velocities computed by an Eulerian flow solver. The filtered scalar values in each cell are constructed by ensemble averaging the particle scalar values in that cell.

In the FDF transport method, the main link between the flow solver and the particle solver is the density field. This field, typically computed from the particle solver, has been the cause of severe numerical difficulties in pressure-based methods because the density field computed from a finite ensemble size of particles is quite noisy. There are several methods available to address this problem. One method is to use density underrelaxation to smooth out the density field. A similar approach was successfully used by Forkel and Janicka[37] in their LES of a turbulent hydrogen diffusion flame with an assumed PDF model. A second method[41] to overcome the problem is to solve the scalar transport equations in addition to the velocity and pressure equations. The filtered reaction rates required in the scalar equations are computed from the particle field. In this approach, the reaction rates are the main link between the flow and particle solvers. The disadvantage of this approach is that a large number of transport equations have to be solved when the number of scalars is large. A third method to overcome numerical difficulties is as suggested by Muradoglu et al.,[66] in a RANS context, in which the transport equation of total sensible internal energy is solved for. The source term in this equation is computed from the particle solver. Filtered density is then computed from an expression that involves mean pressure, total sensible internal energy, and velocities. A fourth method to overcome numerical instabilities is via the solution of the transport equation for

$$\Theta = R^0 \sum \frac{T\phi_\alpha}{M_\alpha}$$

The source terms in this equation are computed from the particle solver. Given $\tilde{\Theta}$, mean density could be easily computed from the relation $\bar{\rho} = \bar{p}/\tilde{\Theta}$.

A few examples of LES of turbulent reacting flows are presented next. The first case presented is the LES of a model gas turbine combustor for which experimental data are presented by Pitsch et al.[67] A schematic of the combustor is shown in Fig. 12. The combustor consists of concentric tubes, with the central tube feeding methane and an outer tube feeding air into a test section. Both the air and fuel are coswirled to provide liftoff of the flame in the test section. The test section terminates into a narrow pipe. LES of the flow are performed using the mixture fraction-based assumed PDF model in conjunction with an equilibrium chemistry description of the flame. Simulations are also performed with the FDF model in conjunction with the Westbrook and Dryer two-step chemistry model. In the FDF solver, combustion chemistry is integrated using a table lookup algorithm. Density is underrelaxed with a factor of 0.001 to stabilize the FDF calculations. This is akin to performing a running time average of the density field over 1000 time steps. In the FDF calculations, 10 particles/cell are used. Inlet boundary conditions for both calculations are taken from a previous simulation of the same combustor.[68] The computational grid for the present calculation consists of 1.1 million grid points and is constructed using O- and H-grid elements. Calculations are performed on six processors. The FDF calculation with the two-step chemistry model is henceforth denoted as FDF/2-step.

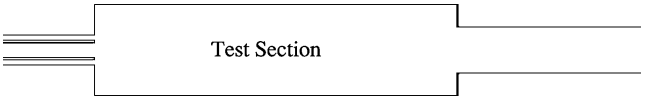

Fig. 12 Schematic of swirl-stabilized model gas turbine combustor.

The swirling flow establishes a recirulating region, which acts as a stabilization mechanism for the flame. Figure 13 shows the mean velocities at several axial locations in the test section. Note that, at $x = 0.043$ m, which is very close to the inlet of the test section, peak velocities are better predicted by the assumed PDF model. Near the centerline, the FDF/2-step model shows better predictions. At $x = 0.115$ m and 0.151 m, the FDF/2-step model shows superior predictions. The rms of the axial velocity is shown in Fig. 14 at several axial locations. At $x = 0.043$ m, both of the models show poor predictions near the centerline. The comparison improves away from the centerline. At $x = 0.115$ and 0.151 m, both models show excellent prediction of fluctuations.

Figure 15 shows the instantaneous temperature fields from the assumed PDF model and the FDF/2-step model. The FDF/2-step model shows a highly lifted flame compared to that shown by the

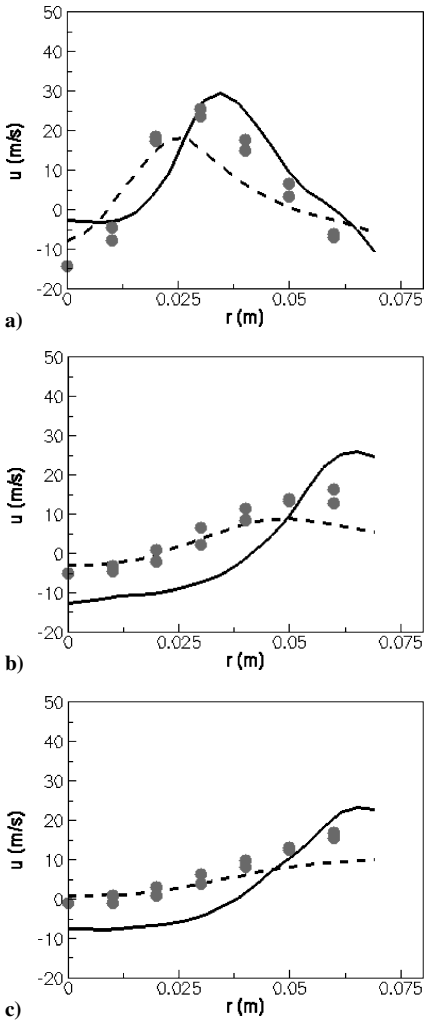

Fig. 13 Mean axial velocities at several axial locations: a) $x = 0.043$ m, b) $x = 0.115$ m, and c) $x = 0.151$ m: ——, assumed PDF model; - - - -, FDF model; and ●, experimental data.

assumed PDF model. Note that with the assumed PDF model, temperatures are higher and the flame shows two tails at the flame stabilization location. The fast burning seen with this model is due to the single variable used to parameterize methane combustion chemistry. A two-variable assumed PDF formulation does not show this behavior.[67]

Detailed comparisons of the mean temperatures at several axial locations are shown in Fig. 16. In Fig. 16, an additional curve is shown for predictions from the FDF method using a detailed 15-step, 21-species chemical kinetics mechanism.[69] Integration of the detailed chemical kinetics scheme is achieved using the in situ adaptive tabulation[70] scheme. Also, in addition to the three LES calculations, results from RANS with a transport PDF model and 2-step chemistry are also shown in Fig. 16.

At $x = 0.043$ m, the FDF/2-step and RANS/PDF models underpredict the temperatures near the centerline significantly. The assumed PDF model shows a temperature spike at $r \sim 0.03$ m,

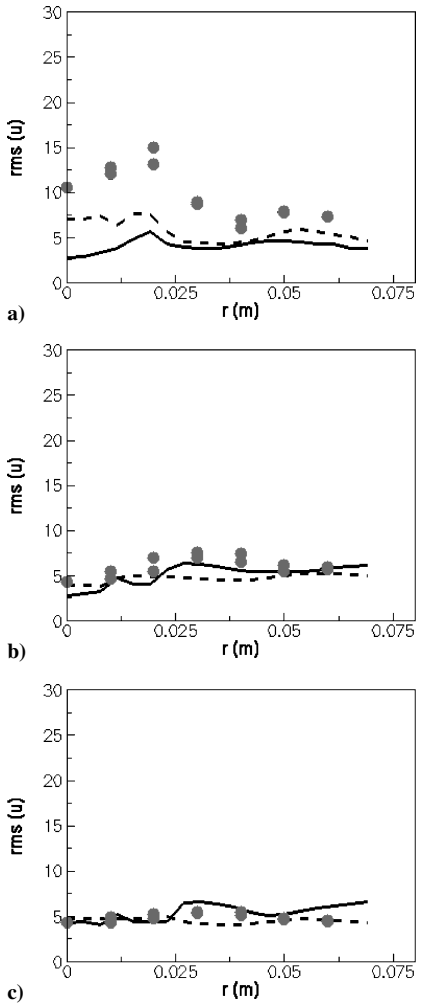

Fig. 14 Axial velocity rms at several axial locations: a) $x = 0.043$ m, b) $x = 0.115$ m, and c) $x = 0.151$ m: ——, assumed PDF model; - - - -, FDF model; and ●, experimental data.

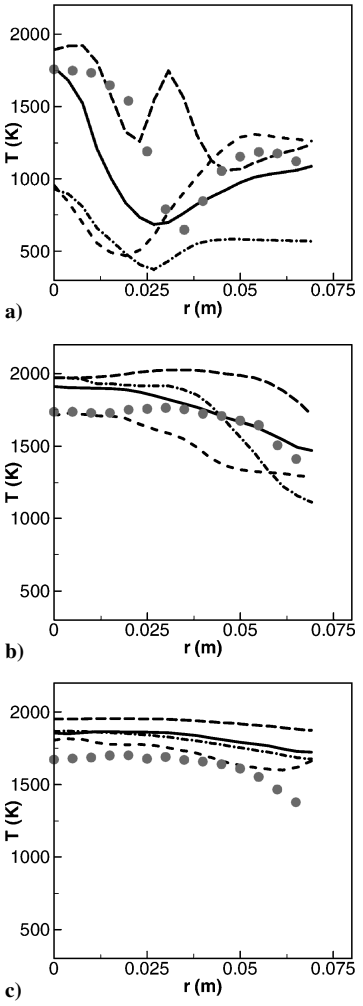

Fig. 16 Mean temperatures at several axial locations: a) $x = 0.043$ m, b) $x = 0.151$ m, and c) $x = 0.26$ m: ——, FDF model with detailed chemical kinetics; — —, assumed PDF model; - - - -, FDF model; —·—, RANS/PDF transport model; ●, experimental data.

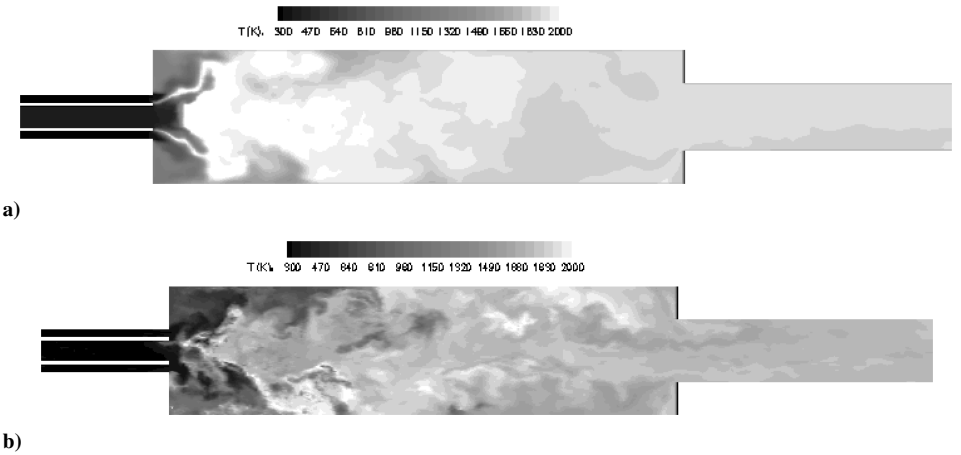

Fig. 15 Instantaneous temperatures in model gas turbine combustor: a) mixture fraction variable-based assumed PDF model in conjunction with equilibrium chemistry used for turbulent combustion and b) FDF turbulent combustion model in conjunction with Westbrook and Dryer two-step methane reaction model.

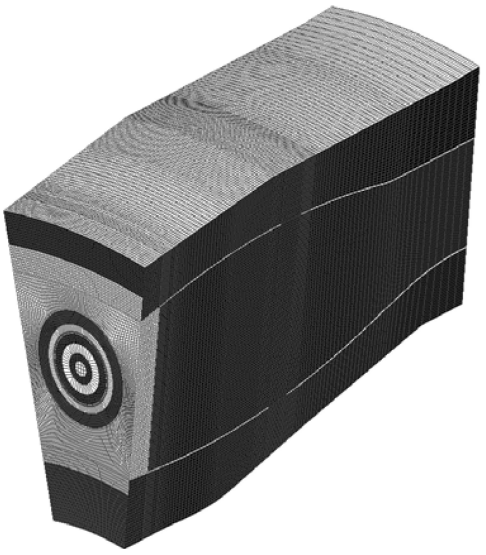

Fig. 17 Computational grid of sector model of developmental gas turbine combustor.

which is an artifact of the single-variable PDF as explained before. The FDF model with detailed chemical kinetics shows reasonable agreement with data. At $x = 0.151$ m, the assumed PDF model consistently overpredicts temperatures. The RANS/PDF and FDF/detailed-chemistry models show higher temperatures near the centerline. Away from the centerline, the FDF/detailed-chemistry model shows good agreement with data. At $x = 0.26$ m, all of the models show overprediction of temperature values. Because radiation is not accounted for in the simulations, this overprediction is expected. These results suggest that the flame is highly lifted in the FDF/2-step and RANS/PDF calculations. Flame liftoff is reasonably predicted using detailed chemical kinetics. At the base of lifted flames, finite-rate chemistry effects are significant. Hence, flame liftoff height is sensitive to the accuracy of the chemical kinetic mechanism and mixing model in FDF (or RANS/PDF) transport calculations. In the present simulations, the two-step mechanism may not be accurate enough to predict the correct flame liftoff height. Deficiences with the IEM mixing model are well known. More accurate mixing models such as the Euclidean minimum spanning tree[71] model may yield better results. Nevertheless, the present calculations demonstrate that LES/FDF calculations of complex flow configurations are feasible.

LES results from a single-sector model of a developmental gas turbine combustor are presented next. The grid for the combustor, presented in Fig. 17, consists of roughly 1 million cells. The combustor model has all of the elements of a practical gas turbine combustor, swirlers, fuel nozzles, primary and dilution holes, cooling flows, etc. Note that the annuli of the combustor and the liner are also included in the computational flow model. The jet-A fuel is simulated using a surrogate two-step Westbrook and Dryer mechanism with propane rate parameters. The localized dynamic and the eddy breakup models are used in the calculations. Figure 18 shows contours of the instantaneous velocity magnitude and temperature fields in the azimuthal centerplane of the combustor. A recirculating zone is seen in the primary zone, which helps to stabilize combustion. High temperatures are seen in the primary zone and also in regions downstream of the dilution holes.

Figure 19 shows the mean exit temperature profiles from calculations and full-annular rig measurements. Also shown in Fig. 19 are profiles from LES calculations of the liner alone (without the annuli), RANS calculations, and rig measurements. Note that LES of the liner plus annuli model and the RANS of the liner-only model show similar profiles. However, LES of the liner-only model show a very different profile. In the liner-only model, no turbulent fluctuations were superimposed on the velocity profiles prescribed at the primary and dilution ports. This may have resulted in overpenetration of the jets from these ports, thus, significantly affecting the exit

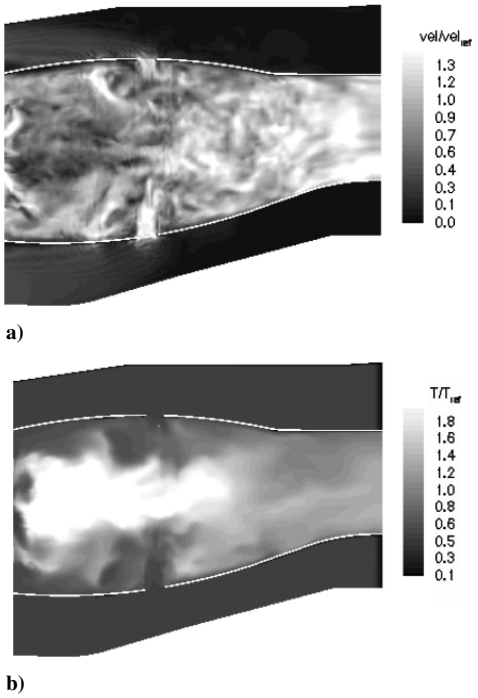

Fig. 18 Developmental gas turbine combustor: a) instantaneous velocity magnitude and b) temperature.

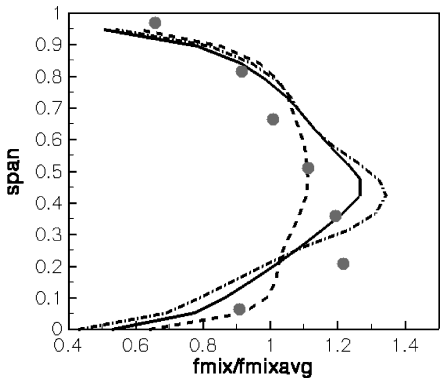

Fig. 19 Mean exit mixture fraction (averaged in circumferential direction) along combustor span: ——, LES of liner plus annuli; - - - -, LES of liner only; —·—, RANS of liner only; and ●, rig measurements.

temperature profile. Note that all of the three calculations predict peak mixture fraction to be at a higher span than that seen in the data. (Subsequent RANS calculations with improved boundary conditions showed excellent agreement with data. It is expected that, with these boundary conditions, the LES calculations will also show improvement.)

The LES solver is also applied to a production combustor shown in Fig. 20. The eddy breakup model and the localized dynamic model are used in the simulation of the flow in this combustor. Figure 21 shows contours of the instantaneous velocity magnitude and temperature in the flowfield. These results again demonstrate that LES of complex gas turbine combustors is feasible.

Future Developments

As LES is applied to increasingly complex problems, there is a need to further enhance the theoretical basis of the LES methodology to improve accuracy. One area that is gaining attention is the explicit filtering approach for LES. An advantage of explicit filtering is that grid-independent LES solutions can be obtained by allowing filters to be chosen independent of the computational mesh. Another advantage is that numerical errors in the high-frequency range can be reduced or eliminated. In the explicit filtering method, an alternative

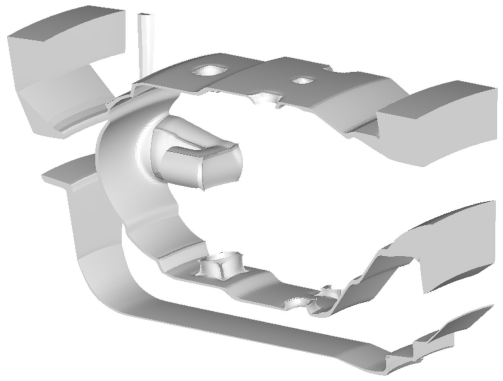

Fig. 20 Model of production combustor for LES; 1-million-element grid.

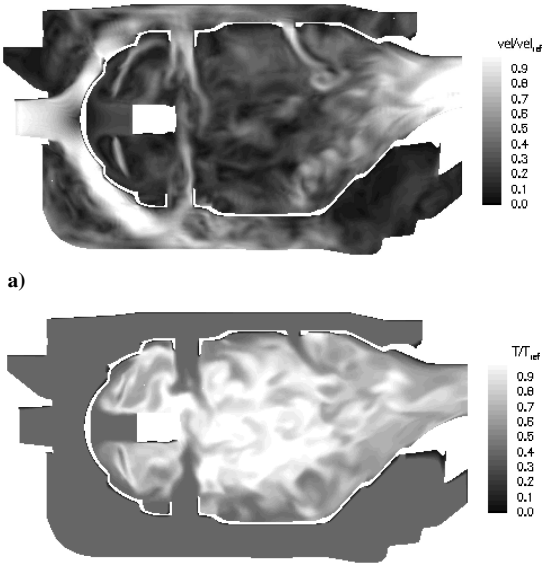

Fig. 21 Production combustor: a) instantaneous velocity magnitude and b) temperature fields.

form of the LES equations is solved.[72] The momentum equations are written as

$$\frac{\partial \overline{u_j}}{\partial t} + \frac{\partial \overline{\bar{u}_i \bar{u}_j}}{\partial x_i} = -\frac{\partial \overline{p}}{\partial x_j} + \frac{\partial \overline{\tau_{ij}}}{\partial x_i} - \frac{\partial T_{ij}}{\partial x_i} \tag{20}$$

and the SGS stress is written as $T_{ij} = \overline{\bar{u}_i \bar{u}_j} - \overline{u_i u_j}$. Note that there is an extra filtering step in the convective terms. The advantage of this is that frequencies higher than the cutoff are not generated by the nonlinear terms. Filters are chosen such that they commute with differentiation. In support of this requirement, a new class of commutative filters has been developed for structured and unstructured grids.[72,73] Further research is required to assess the suitability of explicit filtering methods for large complex problems.

The SGS stress and turbulent-chemistry interactions are the two most important terms to be modeled in LES. New methods such as one-dimensional turbulence,[74] velocity FDF,[64] and SGS estimation methods[33] appear promising for modeling SGS stress. For turbulence–chemistry interactions, the linear-eddy model[75] and the G-equation model[67] are promising avenues that are being explored. The scalar FDF transport method is just beginning to be applied for practical problems. FDF with detailed chemical kinetics could be used to address emissions, extinction, reignition, and lean blowout, issues of importance to the gas turbine community. Further work is needed to exploit the capabilities of the FDF method. In addition to the scalar FDF method, the joint velocity–scalar FDF method has been developed recently.[43] The feasibility of using this method for complex flows needs to be explored. For combustion instabilities, a low-dissipative compressible version of the pressure-based method has to be developed. Some advances are being made to this effect.[76]

The unsteady nature of LES makes it more suited (than RANS) for tackling transient problems such as lean blowout, relight, and combustion instabilities. In recent years, applications of RANS to a variety of steady-state high fuel–air ratio gas turbine combustor flows have highlighted deficiencies with conventional RANS models. There is an increasing desire to use LES for such flows. However, the overall turnaround time of LES is an important issue. Presently, the wall clock time for a typical gas turbine combustor simulation such as those shown in Figs. 17–21 is about four days on an eight-processor LINUX machine. To improve accuracy, grids involving several million cells will have to be used. Correspondingly, CPU requirements are expected to increase significantly. With the development of more efficient solvers and large computing resources becoming more affordable, it is foreseeable that LES may soon become the preferred tool for gas turbine applications.

Conclusions

Although LES is computationally expensive compared to RANS, increasing computing power in conjunction with more accurate results obtained with LES for a variety of benchmark flows is making LES attractive for gas turbine combustor applications. In this paper, an overview of recent activities related to LES being pursued by the authors at Rolls–Royce is presented. The state of the art of LES for gas turbine combustion systems is reviewed. Numerical and modeling issues are presented, and some promising models are discussed. A hierarchy of validation cases performed on several nonreacting and reacting benchmark flows are presented. These cases ranging from simple lid-driven cavity flow to complex gas turbine combustor flow highlight the predictive capabilities of LES. As LES is applied to more complex problems, more validation and verification efforts are needed to assess the limitations and accuracy of the submodels. Further improvement to the underlying theoretical foundation of LES is mandated to improve accuracy. A key issue for LES to be accepted as a practical design tool in industry is the turnaround time. Efficient solvers with parallel processing capabilities in conjunction with large computational resources will help overcome this barrier.

Acknowledgments

This work was funded in part by a grant from the Indiana State 21st Century Research and Technology Fund. The authors acknowledge the contributions of Nagendra Dittakavi of Purdue University to the simulations of the lid-driven cavity and plane turbulent Couette cases presented in Figs. 1–4.

References

[1]Mahesh, K., Constantinescu, G., and Moin, P., "LES of Gas Turbine Combustors," *Annual Research Briefs*, Center for Turbulence Research, Stanford Univ. and NASA Ames Research Center, 2000, pp. 219–228.

[2]Kim, W. W-., Menon, S., and Mongia, H. C., "Large-Eddy Simulation of a Gas Turbine Combustor Flow," *Combustion Science and Technology*, Vol. 143, No. 1–6, 1999, pp. 25–62.

[3]Selle, L., Lartigue, G., Poinsot, T., Kaufmann, P., Krebs, W., and Veynante, D., "Large-Eddy Simulation of Turbulent Combustion for Gas Turbines with Reduced Chemistry," *Proceedings of the Summer Program*, Center for Turbulence Research, Stanford Univ. and NASA Ames Research Center, 2002, pp. 333–344.

[4]Cannon, S. M., Smith, C. E., and Anand, M. S., "LES Predictions of Combustor Emissions in an Aero Gas Turbine Engine," AIAA Paper 2003-4521, July 2003.

[5]Leonard, A., "Energy Cascade in Large Eddy Simulations of Turbulent Fluid Flows," *Advances in Geophysics A*, Vol. 18, 1974, p. 237.

[6]Aldama, A. A., "Filtering Techniques for Turbulent Flow Simulation," *Lecture Notes in Engineering*, Vol. 49, Springer-Verlag, New York, 1990.

[7]Ghosal, S., and Moin, P., "The Basic Equations for the Large Eddy Simulation of Turbulent Flows in Complex Geometry," *Journal of Computational Physics*, Vol. 118, No. 1, 1995, pp. 24–37.

[8]Anand, M. S., Zhu, J., Connor, C., and Razdan, M. K., "Combustor Flow Analysis Using an Advanced Finite-Volume Design System," American Society of Mechanical Engineers, ASME Paper 99-GT-273, June 1999.

[9]Mittal, R., and Moin, P., "Suitability of Upwind-Biased Finite Difference Schemes for Large-Eddy Simulation of Turbulent Flows," *AIAA Journal*, Vol. 35, No. 8, 1997, pp. 1415–1417.

[10]Morinishi, Y., Lund, T. S., Vasilyev, O. V., and Moin, P., "Fully Conservative Higher Order Finite Difference Schemes for Incompressible Flows," *Journal of Computational Physics*, Vol. 143, June 1998, pp. 90–124.

[11]Vasilyev, O. V., "High Order Finite Difference Schemes on Non-Uniform Meshes with Good Conservation Properties," *Journal of Computational Physics*, Vol. 157, Jan. 2000, pp. 746–761.

[12]Mahesh, K., Constantinescu, G., and Moin, P., "A Numerical Method for Large-Eddy Simulation in Complex Geometries," *Journal of Computational Physics*, Vol. 197, June 2004, pp. 215–240.

[13]Benhamadouche, S., Mahesh, K., and Constantinescu, G., "Collocated Finite-Volume Schemes for Large-Eddy Simulation on Unstructured Meshes," *Proceedings of the Summer Program*, Center for Turbulence Research, Stanford Univ. and NASA Ames Research Center, 2002, pp. 143–154.

[14]Pierce, C. D., and Moin, P., "Progress-Variable Approach for Large Eddy Simulation of Turbulent Reacting Flows," Dept. of Mechanical Engineering, Rept. TF-80, Stanford Univ., Stanford, CA, June 2001.

[15]Rhie, C. M., and Chow, W. L., "A Numerical Study of the Turbulent Flow past an Isolated Airfoil with Trailing Edge Separation," *AIAA Journal*, Vol. 21, 1983, pp. 1525–1532.

[16]Pope, S. B., "Ten Questions Concerning the Large-Eddy Simulation of Turbulent Flows," *New Journal of Physics*, Vol. 6, March 2004, p. 35.

[17]Zhu, J., "On the Higher-Order Bounded Discretization Schemes for Finite-Volume Computations of Incompressible Flows," *Computer Methods in Applied Mechanics and Engineering*, Vol. 98, No. 3, 1992, pp. 345–360.

[18]Patankar, S. V., *Numerical Heat Transfer and Fluid Flow*, McGraw–Hill, New York, 1980.

[19]Smagorinsky, J., "General Circulation Experiments with the Primitive Equations, Part I: The Basic Experiment," *Monthly Weather Review*, Vol. 91, No. 3, 1963, pp. 99–164.

[20]Germano, M., Piomelli, U., Moin, P., and Cabot, W. H., "A Dynamic Subgrid-Scale Eddy Viscosity Model," *Physics of Fluids A*, Vol. 3, No. 7, 1991, pp. 1760–1765.

[21]Piomelli, U., and Liu, J., "Large-Eddy Simulation of Rotating Channel Flows Using a Localized Dynamic Model," *Physics of Fluids*, Vol. 7, No. 4, 1995, pp. 839–848.

[22]Ghosal, S., Lund, T. S., Moin, P., and Akselvoll, K., "A Dynamic Localization Model for Large-Eddy Simulation of Turbulent Flows," *Journal of Fluid Mechanics*, Vol. 286, 1995, pp. 229–255.

[23]Meneveau, C., Lund, T., and Cabot, W., "A Lagrangian Dynamic Subgrid-Scale Model of Turbulence," *Journal of Fluid Mechanics*, Vol. 319, 1996, pp. 353–385.

[24]Porte-Agel, F., Meneveau, C., and Parlange, M. B., "A Scale-Dependent Dynamic Model for Large-Eddy Simulation: Application to a Neutral Atmospheric Boundary Layer," *Journal of Fluid Mechanics*, Vol. 415, 2000, pp. 261–284.

[25]Kim, W. W., and Menon, S., "An Unsteady Incompressible Navier–Stokes Solver for Large Eddy Simulation of Turbulent Flows," *International Journal for Numerical Methods in Fluids*, Vol. 31, No. 6, 1999, pp. 983–1017.

[26]Prasad, A. K., and Koseff, J. R., "Reynolds Number and End-Wall Effects on a Lid-Driven Cavity Flow," *Physics of Fluids A*, Vol. 1, Feb. 1989, pp. 208–218.

[27]Bech, K. H., Tillmark, N., Alfredsson, P. J., and Andersson, H. I., "An Investigation of Turbulent Plane Couette Flow at Low Reynolds Numbers," *Journal of Fluid Mechanics*, Vol. 286, 1995, pp. 291–325.

[28]Aydin, E. M., and Leutheusser, H. J., "Experimental Investigation of Turbulent Plane Couette Flow," *ASME Forum on Turbulent Flows*, FED Vol. 51, American Society of Mechanical Engineers, Cincinnati, OH, 1987, p. 51.

[29]Sommerfeld, M., and Qiu, H. H., "Experimental Studies of Spray Evaporation in Turbulent Flow," *International Journal of Heat and Fluid Flow*, Vol. 19, 1998, pp. 10–22.

[30]Bardina, J., "Improved Turbulent Models Based on Large Eddy Simulation of Homogeneous, Incompressible, Turbulent Flows," Ph.D. Dissertation, Mechanical Engineering Rept. TF-19, Stanford Univ., Stanford, CA, 1983.

[31]Liu, S. W., Meneveau, C., and Katz, J., "On the Properties of Similarity Subgrid Scale Models as Deduced from Measurements in Turbulent Jets," *Journal of Fluid Mechanics*, Vol. 275, 1994, p. 83.

[32]Adams, N. A., and Stolz, S., "Deconvolution Methods for Subgrid-Scale Approximation in Large-Eddy Simulation," *Modern Simulation Strategies for Turbulent Flow*, edited by B. Geurts, Edwards, Ann Arbor, MI, 2001, pp. 21–41.

[33]Domaradski, J. A., and Adams, N. A., "Direct Modeling of Subgrid Scales of Turbulence in Large Eddy Simulation," *Journal of Turbulence*, Vol. 3, No. 24, 2002, pp. 1–19.

[34]Sagaut, P., *Large Eddy Simulations for Incompressible Flows*, Springer-Verlag, Berlin, 2001.

[35]Meneveau, C., and Katz, J., "Scale-Invariance and Turbulence Models for Large Eddy Simulation," *Annual Review of Fluid Mechanics*, Vol. 32, 2000, pp. 1–32.

[36]Cook, A. W., and Riley, J. J., "A Subgrid Model for Equilibrium Chemistry in Turbulent Flows," *Physics of Fluids A*, Vol. 6, No. 8, 1994, pp. 2868–2870.

[37]Forkel, H., and Janicka, J., "Large Eddy Simulation of a Turbulent Hydrogen Diffusion Flame," *Flow, Turb. and Comb*, Vol. 65, No. 2, 2000, pp. 163–175.

[38]Steiner, H., and Pitsch, H., "Large-Eddy Simulation of a Turbulent Piloted Methane/Air Diffusion Flame (Sandia Flame D)," *Physics of Fluids*, Vol. 12, No. 10, 2000, pp. 2541–2554.

[39]Pierce, C. D., and Moin, P., "Large Eddy Simulation of a Confined Coaxial Jet with Swirl and Heat Release," AIAA Paper 98-2892, June 1998.

[40]Jones, W. P., and Branley, N., "Large Eddy Simulation of a Turbulent Non-Premixed Flame," Proceedings of the 11th Symposium on Turbulent Shear Flows, Grenoble, France, 1997.

[41]James, S., and Jaberi, F. A., "Large Scale Simulations of Two-Dimensional Non-Premixed Methane Jet Flames," *Combustion and Flame*, Vol. 123, No. 4, 2000, pp. 465–487.

[42]Moin, P., Squires, K., Cabot, W., and Lee, S., "A Dynamic Subgrid-Scale Model for Compressible Turbulence and Scalar Transport," *Physics of Fluids A*, Vol. 3, Nov. 1991, pp. 2746–2757.

[43]Sheikhi, R. M. H., Drozda, T. G., Givi, P., and Pope, S. B., "Velocity-Scalar Filtered Density Function for Large Eddy Simulation of Turbulent Flows," *Physics of Fluids*, Vol. 15, No. 8, 2003, pp. 2321–2337.

[44]Gosman, A. D., and Ioannides, E., "Aspects of Computer Simulation of Liquid Fueled Combustors," AIAA Paper 81-0323, Jan. 1981.

[45]Crowe, C., Sommerfeld, M., and Tsuji, Y., *Multiphase Flows with Droplets and Particles*, CRC Press, Boca Raton, FL, 1997.

[46]Pannala, S., and Menon, S., "Large Eddy Simulations of Two-Phase Turbulent Flows," AIAA Paper 98-0163, Jan. 1999.

[47]Miller, R. S., and Bellan, J., "Direct Numerical Simulation and Subgrid Analysis of a Transitional Droplet Laden Mixing Layer," *Physics of Fluids*, Vol. 12, No. 3, 2000, pp. 650–671.

[48]Apte, S. V., Mahesh, K., Moin, P., and Oefelein, J. C., "Large-Eddy Simulation of Swirling Particle-Laden Flows in a Coaxial-Jet Combustor," *International Journal of Multiphase Flow*, Vol. 29, 2003, pp. 1311–1331.

[49]Chin, J. S., and Lefebvre, A. H., "The Role of the Heat-Up Period in Fuel Drop Evaporation," *International Journal of Turbo Jet Engines*, Vol. 2, 1985, pp. 315–325.

[50]Custer, J. R., and Rizk, N. K., "Effect of Fuel Nozzle Concept on Spray Quality and Droplet Size Distribution," AIAA Paper 85-1186, July 1985.

[51]Cha, C., Zhu, J., and Anand, M. S., "A Comprehensive Liquid Fuel Spray Injection Model for CFD Simulations of Gas Turbine Combustors," AIAA Paper 2005-0349, Jan. 2005.

[52]Ham, F., Apte, S., Iaccarino, G., Wu, X., Herrmann, M., Constantinescu, G., Mahesh, K., and Moin, P., "Unstructured LES of Reacting Multiphase Flows in Realistic Gas Turbine Combustors," *Annual Research Briefs*, Center for Turbulence Research, Stanford Univ. and NASA Ames Research Center, 2003, pp. 139–160.

[53]James, S., Anand, M. S., and Pope, S. B., "The Lagrangian PDF Method for Gas Turbine Combustor Flows," AIAA Paper 2002-4017, July 2002.

[54]Fureby, C., and Lofstrom, C., "Large-Eddy Simulations of Bluff-Body Stabilized Flames," *Twenty-Fifth Symposium (International) on Combustion*, Combustion Inst., Pittsburgh, PA, 1994, pp. 1257–1264.

[55]Branley, N., and Jones, W. P., "Large Eddy Simulation of a Turbulent Non-Premixed Flame," *Combustion and Flame*, Vol. 127, No. 1–2, 2001, pp. 1914–1934.

[56]Pierce, C. D., and Moin, P., "Progress-Variable Approach for Large-Eddy Simulation of Nonpremixed Turbulent Combustion," *Journal of Fluid Mechanics*, Vol. 504, 2004, pp. 73–97.

[57]Pierce, C. D., and Moin, P., "A Dynamic Model for Subgrid-Scale Variance and Dissipation Rate of a Conserved Scalar," *Physics of Fluids*, Vol. 10, No. 12, 1998, pp. 3041–3044.

[58]Ihme, M., Cha, C., and Pitsch, H., "Prediction of Local Extinction and Reignition Effects in Non-Premixed Turbulent Combustion Using a Flamelet/Progress Variable Approach," *Thirtieth Symposium (International) on Combustion*, Combustion Inst., Pittsburgh, PA, 2004, pp. 793–800.

[59]Bushe, W. K., and Steiner, H., "Conditional Moment Closure for Large Eddy Simulation of Nonpremixed Turbulent Reacting Flows," *Physics of Fluids*, Vol. 11, No. 7, 1999, pp. 1896–1906.

[60]James, S., and Jaberi, F. A., "A Dynamic Similarity Model for Large Eddy Simulation of Turbulent Combustion," *Physics of Fluids*, Vol. 10, No. 7, 1998, pp. 1775–1777.

[61]DesJardin, P. E., and Frankel, S. H., "Large Eddy Simulation of a Turbulent Non-Premixed Reacting Jet: Application and Assessment of Subgrid-Scale Combustion Models," *Physics of Fluids*, Vol. 10, No. 9, 1998, pp. 2298–2314.

[62]Colucci, P. J., Jaberi, F. A., Givi, P., and Pope, S. B., "Filtered Density Function for Large Eddy Simulation of Turbulent Reacting Flows," *Physics of Fluids*, Vol. 10, No. 2, 1998, pp. 499–515.

[63]Jaberi, F. A., Colucci, P. J., James, S., Givi, P., and Pope, S. B., "Filtered Mass Density Function for Large Eddy Simulation of Turbulent Reacting Flows," *Journal of Fluid Mechanics*, Vol. 401, 1999, pp. 85–121.

[64]Gicquel, L. Y. M., Givi, P., Jaberi, F. A., and Pope, S. B., "Velocity Filtered Density Function for Large Eddy Simulation of Turbulent Flows," *Physics of Fluids*, Vol. 14, No. 3, 2002, pp. 1196–1213.

[65]Givi, P., "Subgrid Scale Modeling in Turbulent Combustion: A Review," AIAA Paper 2003-5081, July 2003.

[66]Muradoglu, M., Jenny, P., Pope, S. B., and Caughey, D. A., "A Consistent Hybrid Finite-Volume/Particle Method for the PDF Equations of Turbulent Reactive Flows," *Journal of Computational Physics*, Vol. 154, No. 2, 1999, pp. 342–371.

[67]Pitsch, H., Trouillet, P., Pierce, C. D., Tribbett, E., Sipperley, C. M., Edwards, C. F., and Bowman, C. T., "A Joint Experimental/Large-Eddy Simulation Study of a Model Gas Turbine Combustor," Western States Section of the Combustion Inst., Paper WSS-02S31, March 2002.

[68]Dittakavi, N., Khosla, S., Eriksen, M., Chandy, A., Gore, J. P., and Frankel, S. H., "Numerical Modeling of Nonreacting and Reacting Swirl Combustors: Key Issues and Validation Studies," *Proceedings of the Third Joint Meeting of the U.S. Sections of the Combustion Institute*, Combustion Inst., Pittsburgh, PA, 2003.

[69]Sung, C. J., Law, C. K., and Chen, J. Y., "An Augmented Reduced Mechanism for Methane Oxidation with Comprehensive Global Parametric Validation," *Twenty-Seventh Symposium (International) on Combustion*, Combustion Inst., Pittsburgh, PA, 1998, pp. 295–304.

[70]Pope, S. B., "Computationally Efficient Implementation of Combustion Chemistry Using an In Situ Adaptive Tabulation," *Combustion Theory and Modelling*, Vol. 1, Jan. 1997, pp. 41–63.

[71]Subramanium, S., and Pope, S. B., "A Mixing Model for Turbulent Reactive Flows Based on Euclidean Minimum Spanning Tree," *Combustion and Flame*, Vol. 115, No. 4, 1998, pp. 487–514.

[72]Vasilyev, O., Lund, T., and Moin, P., "A General Class of Commutative Filters for LES in Complex Geometries," *Journal of Computational Physics*, Vol. 146, No. 1, 1998, pp. 105–123.

[73]Marsden, A., Vasilyev, O., and Moin, P., "Construction of Commutative Filters for LES on Unstructured Meshes," *Annual Research Briefs*, Center for Turbulence Research, Stanford Univ. and NASA Ames Research Center, 2000, pp. 179–192.

[74]Kerstein, A. R., "One-Dimensional Turbulence: Model Formulation and Application to Homogeneous Turbulence, Shear Flows, and Buoyant Stratified Flows," *Journal of Fluid Mechanics*, Vol. 392, 1999, p. 277.

[75]Menon, S., McMurtry, P. A., and Kerstein, A. R., "A Linear-Eddy Subgrid Model for Turbulent Combustion," *Large Eddy Simulation of Complex Engineering and Geophysical Flows*, edited by B. Galperin and S. A. Orszag, Cambridge Univ. Press, 1993, Chap. 14, pp. 287–314.

[76]Wall, C., Pierce, C. D., and Moin, P., "A Semi-Implicit Method for Resolution of Acoustic Waves in Low Mach Number Flows," *Journal of Computational Physics*, Vol. 181, No. 2, 2002, pp. 545–563.

J. C. Oefelein
Guest Editor